

# Beamforming Gain Maximization for Fluid Reconfigurable Intelligent Surface: A Minkowski Geometry Approach

Hong-Bae Jeon, *Member, IEEE*

arXiv:2602.11654v1 [eess.SP] 12 Feb 2026

**Abstract**—This paper investigates beamforming-gain maximization for a fluid reconfigurable intelligent surface (FRIS)-assisted downlink system, where each active port applies a finite-resolution unit-modulus phase selected from a discrete codebook. The resulting design couples the multi-antenna base-station (BS) beamformer with combinatorial FRIS port selection and discrete phase assignment, leading to a highly nonconvex mixed discrete optimization. To address this challenge, we develop an alternating-optimization (AO) framework that alternates between a closed-form maximum-ratio-transmission (MRT) update at the BS and an optimal FRIS-configuration update. The key step of the proposed FRIS configuration is a Minkowski-geometry reformulation of the FRIS codebook superposition: by convexifying the feasible reflected-sum set and exploiting support-function identities, we convert the FRIS subproblem into a one-dimensional maximization over a directional parameter. For each direction, the optimal configuration is obtained constructively via per-port directional scoring, Top- $M_o$  port selection, and optimal codeword assignment. For the practically important regular  $M_p$ -gon phase-shifter codebook, we further derive closed-form score expressions and establish a piecewise-smooth structure of the resulting support function, which leads to a finite critical-angle search that provably identifies the global optimum without exhaustive angular sweeping. Simulation results demonstrate that the proposed framework consistently outperforms benchmarks, achieves near-optimal beamforming gains in exhaustive-search validations, accurately identifies the optimal direction via support-function maximization, and converges rapidly within a few AO iterations.

**Index Terms**—Fluid reconfigurable intelligent surface (FRIS), Minkowski sum, convex geometry, alternating optimization.

## I. INTRODUCTION

THE continuing evolution of wireless communications is being accelerated by an unprecedented demand for extremely high data rates, ultra-reliable transmission, and low-latency connectivity, driven by the proliferation of data-intensive and latency-critical services [1]–[4]. To accommodate these stringent requirements, sixth-generation (6G) wireless systems are envisioned to transcend traditional link-level design and adopt new paradigms that simultaneously address spectral-efficiency [5], interference mitigation in ultra-dense deployments [6], and communication reliability under high mobility and adverse propagation environments [7], [8]. Meanwhile, these ambitious performance targets must be achieved

This work was supported by Hankuk University of Foreign Studies Research Fund of 2026. (Corresponding Author: Hong-Bae Jeon)

H.-B. Jeon is with the Department of Information Communications Engineering, Hankuk University of Foreign Studies, Yong-in, 17035, Korea (e-mail: hongbae08@hufs.ac.kr).

under tight constraints on energy consumption and hardware complexity, necessitating fundamentally new approaches to wireless system architecture and signal processing.

In this context, the ability to actively reconfigure the wireless propagation environment has emerged as a key enabler for 6G networks [9]. Rather than treating the radio environment as an uncontrollable and often hostile medium, future wireless systems are envisioned to incorporate intelligent, environment-aware components that can adaptively shape signal propagation to improve coverage, reliability, and energy-efficiency [10], [11]. This paradigm shift has naturally led to the development of reconfigurable intelligent surfaces (RIS), which provide a scalable and cost-effective means of manipulating electromagnetic waves through the electronic control of a large number of low-cost reflecting elements [12], [13].

By appropriately adjusting the phase responses, RIS-assisted systems can coherently combine the reflected signals with the direct path, thereby enhancing the received signal strength and coverage without requiring additional radio-frequency chains at the surface [14], [15]. Owing to this appealing property, RIS have attracted considerable attention as an energy- and cost-efficient alternative to conventional relaying architectures [16], [17]. Despite these advantages, conventional RIS architectures are inherently passive and rely on reflecting elements with fixed physical locations. As a result, their achievable performance gains are fundamentally constrained by the severe double-fading attenuation of cascaded channels [18], particularly under unfavorable propagation conditions such as blockage or large path loss [17], [19]. Moreover, the lack of position reconfigurability limits the ability of RIS to fully adapt to channel variations, even when sophisticated phase optimization techniques are employed.

To overcome the rigidity of fixed-position RIS, fluid reconfigurable intelligent surfaces (FRIS) have been introduced [20], [21], inspired by fluid [22]–[24] and reconfigurable [25], [26] antenna systems. In FRIS, the surface is equipped with a dense grid of candidate ports, among which only a subset is dynamically selected. This port-selection capability provides an additional spatial degree-of-freedom (DoF) beyond phase control, enabling the system to exploit location diversity and to form more favorable cascaded channels by selecting effective ports from a large candidate set [27], [28]. Therefore, FRIS has attracted growing research interest, and a variety of studies have been conducted to investigate its performance limits, practical architectures, and optimization strategies under different system settings.

In early studies on FRIS, the authors of [20] and [29] provided initial insights into the performance analysis and enhancement potential of FRIS by introducing position reconfigurability. Specifically, [20] demonstrated notable performance gains over conventional RIS in both single and multi-user scenario through joint optimization framework, while [29] presented analytical characterizations of outage probability and capacity with its tight upper-bound under statistical channel models. Building on this concept, [27] investigated practical FRIS architectures with on/off port selection and discrete phase shifts, showing that selecting a subset of ports can significantly improve link performance while reducing hardware overhead. Recently, [30] explored FRIS in ambient backscatter communication systems, where optimizing the positions of fluid elements was shown to effectively mitigate the double-fading effect of cascaded links and significantly improve the achievable backscatter rate compared to conventional RIS-based designs. The potential of FRIS in secure communications was further explored in [28] and [31], where FRIS-assisted systems were shown to substantially enhance secrecy performance under spatial correlation and partial selection of ports. More recently, extensions such as element-level pattern reconfigurability [32] have been proposed to further enlarge the design space by jointly optimizing radiation patterns and beamforming. Together, these works clearly demonstrate the performance gains achievable by FRIS.

However, practical FRIS implementations are inevitably subject to stringent hardware constraints, under which each activated port can typically apply only a finite-resolution, unit-modulus phase coefficient [27], [32]. Under these constraints, FRIS configuration gives rise to a mixed discrete optimization over the selected-port index set and the discrete phase codewords, which is further coupled with the multi-antenna base-station (BS) beamformer through the resulting effective channel gain [33], [34]. Owing to this strong coupling, direct joint optimization is generally intractable, and a variety of algorithmic approaches have been proposed [20], [27], [28], [30], [31]. Nevertheless, many existing methods rely on restrictive assumptions or structural simplifications to render the problem tractable. In particular, some approaches are limited to uniform-linear-array (ULA) FRIS configurations [28], while others simplify the problem structure by assuming a single-antenna BS [27], [30], [31] or by adopting idealized continuous phase-shift models that are not practically realizable under finite-resolution hardware constraints [20], [30], [31]. Moreover, the direct BS-user link is often ignored [20], [27], [30], [31], or the resulting designs provide no guarantees on near-optimality [20], [27], [28], [30], [31]. Although these methods can achieve reasonable performance through iterative procedures, they suffer from several limitations by relying on simplifying assumptions that assume single-antenna BS or decouple FRIS port selection from discrete phase quantization and thus fail to reflect their inherent realistic joint structure. A summary of the key assumptions and limitations of existing FRIS-related works is provided in Table I. Consequently, the fundamental geometry governing FRIS signal combining under multi-antenna systems and practical hardware constraints remains insufficiently characterized, leaving the underlying

TABLE I  
COMPARISON OF FRIS-RELATED WORKS

Factor	[20]	[27]	[28]	[30]	[31]	Our work
Multi-antenna BS	✓	✗	✓	✗	✗	✓
Non-ULA FRIS structure	✓	✓	✗	✓	✓	✓
Finite-resolution phase codebooks	✗	✓	✓	✗	✗	✓
Analysis with direct link	✗	✗	✓	✗	✗	✓
Near-optimality verification	✗	✗	✗	✗	✗	✓

unified structure of the FRIS configuration problem largely unexplored.

Motivated by these challenges, this paper investigates the beamforming-gain maximization problem in an FRIS-assisted downlink system under multi-antenna BS and practical finite-resolution phase constraints, from a geometric perspective grounded in Minkowski-sum representations of FRIS codebook spaces superpositioned by channel coefficients [35], [36]. By explicitly accounting the MRT architecture at BS and for the fluidic and discrete-phase hardware constraint, the resulting design problem becomes a mixed discrete optimization over port indices, phase codewords, and the transmit beamformer. As a result, the proposed framework reveals a fundamental geometric structure underlying FRIS signal combining and enables an optimal, fully constructive configuration via support-function maximization. In particular, for the practically important regular  $M_p$ -gon phase-shifter codebook, this structure further leads to closed-form per-port scoring and a finite candidate-angle search that provably identifies the global optimum without exhaustive angular sweeping. The main contributions of this work are summarized as follows:

- **Problem formulation with practical FRIS hardware constraints:** We formulate a beamforming-gain maximization problem for an FRIS-assisted downlink system, where the BS beamformer, the selected-port set, and the finite-resolution unit-modulus phase coefficients are jointly optimized. The resulting objective tightly couples continuous beamforming with combinatorial port selection and discrete codeword assignment, yielding a highly nonconvex mixed discrete optimization.
- **Minkowski-geometry reformulation and an optimal FRIS-update subroutine:** To tackle the above coupling, we develop a convex-geometry-based FRIS optimization principle by representing the feasible reflected-sum as a union of Minkowski sums and then convexifying it without loss of optimality. By leveraging support-function identities, we transform the FRIS configuration subproblem into a one-dimensional maximization over a directional parameter. Herein for each candidate direction, the optimal FRIS configuration can be obtained in a fully constructive manner. Specifically, we first compute a direction-dependent score for every candidate port that quantifies its best possible contribution along the given direction under the available discrete phase codewords. We then select the ports with the largest scores. For

the selected ports, we assign the phase codeword that maximizes the directional contribution. Finally, we repeat this procedure over candidate directions and choose the direction that yields the largest overall support value, which directly determines the resulting selected-port set and the corresponding quantized phase coefficients.

- **Specialization to regular  $M_p$ -gon codebooks:** For the practically important regular  $M_p$ -gon phase-shifter codebook, we derive closed-form expressions for the per-port directional scores and establish a nearest-grid codeword selection rule. Exploiting the symmetric structure of the regular  $M_p$ -gon, the resulting closed-form score expressions provide clear analytical and geometrical insight into the impact of finite phase resolution compared to general finite codebooks. Moreover, this specialization reveals a piecewise-smooth structure of the resulting support function, which enables a finite candidate-angle maximization procedure that avoids exhaustive one-dimensional search while provably identifying the global optimum.
- **AO framework with closed-form MRT update and monotonic convergence:** Building on the above FRIS-update subroutine, we develop an AO framework that alternates between a closed-form MRT beamformer update, and an optimal FRIS configuration update that solves the discrete port-selection and phase-quantization step via the proposed support-function maximization. Since each block optimizes the objective with the other block fixed, the objective sequence is guaranteed to be nondecreasing and hence convergent.
- **Performance, near-optimality, and practical behavior validation:** Extensive simulations demonstrate that the proposed framework consistently outperforms conventional baselines across a wide range of system parameters. Furthermore, exhaustive-search validations confirm that the proposed design achieves near-optimal beamforming gains. In addition, the results explicitly illustrate how the optimal FRIS configuration is determined through the proposed support-function-based directional search, validating the effectiveness of the one-dimensional phase optimization procedure. Finally, convergence plots verify that the AO algorithm saturates within only a few iterations, implying that the required iteration count is typically very small, so that the practical computational burden is mainly governed by the structural system parameters rather than by iterative convergence.

*To the best of our knowledge, this work is the first to reveal a fundamental geometric interpretation of FRIS signal combining under finite-resolution phase constraints, showing that fluid port selection induces a convex Minkowski structure that can be optimally exploited via support functions. This leads to a principled AO design with fast convergence, low effective complexity, and consistent performance gains over benchmarks.*

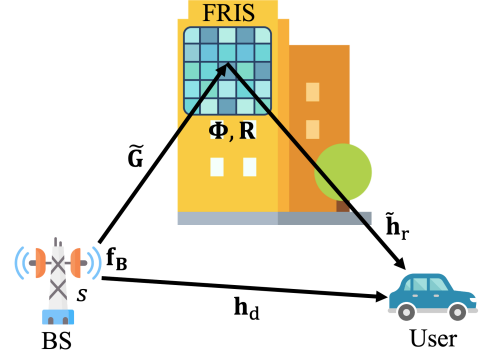


Fig. 1. FRIS-assisted downlink system.

## II. SYSTEM MODEL

### A. Signal Model

As depicted in Fig. 1, we consider a downlink system in which an  $N$ -antenna BS serves a single-antenna user with the aid of an FRIS. The BS transmits a unit-power symbol  $s$  using a beamformer  $\mathbf{f}_B \in \mathbb{C}^N$  under the power constraint

$$\|\mathbf{f}_B\|_2^2 \leq P. \quad (1)$$

The FRIS consists of  $M = M_x \times M_x$  reflective elements uniformly arranged on a square surface of size  $W_x \lambda \times W_x \lambda$ , where  $\lambda$  is the carrier wavelength and  $W_x$  denotes the aperture size normalized by  $\lambda$ . The corresponding inter-element spacing is  $d = \frac{W_x \lambda}{M_x}$ . Accordingly, the FRIS configuration is described by  $\mathbf{w} = [w_1 \cdots w_M]^T$  subject to the  $M_o$ -sparsity constraint [27], [28]

$$|\{m \in \{1, \dots, M\} : w_m \neq 0\}| = M_o, \quad (2)$$

where  $w_m \neq 0$  indicates that port  $m$  is selected. Let  $\mathbf{p}_m$  denote the position of the  $m$ th FRIS candidate port. Due to the close spacing between the elements, we model spatial correlation under isotropic scattering via the zeroth-order spherical Bessel function  $j_0(x)$  [27], [29], [37]. Thereby, we can define the FRIS correlation matrix  $\mathbf{R} \succeq 0$  as

$$[\mathbf{R}]_{m,i} = j_0\left(\frac{2\pi}{\lambda}\|\mathbf{p}_m - \mathbf{p}_i\|_2\right). \quad (3)$$

Let  $\tilde{\mathbf{G}} \in \mathbb{C}^{M \times N}$  and  $\tilde{\mathbf{h}}_r \in \mathbb{C}^M$  have Rician and Rayleigh fading under rich scattering conditions, respectively [28]. We then model the BS-FRIS and the FRIS-user channel as

$$\mathbf{G} = \mathbf{R}^{1/2} \tilde{\mathbf{G}}, \quad \mathbf{h}_r = \mathbf{R}^{1/2} \tilde{\mathbf{h}}_r, \quad (4)$$

respectively, and the direct BS-user channel is denoted by  $\mathbf{h}_d \in \mathbb{C}^N$ , which also follows Rayleigh fading under rich scattering conditions [28]. We assume that the BS has access to perfect channel state information (CSI) for all involved links during the optimization process [21]. Thereby, the received signal  $y$  is expressed as

$$y = (\mathbf{h}_d^* \mathbf{f}_B + \mathbf{h}_r^* \Phi \mathbf{G} \mathbf{f}_B) s + n = \mathbf{a}^* \mathbf{f}_B s + n, \quad (5)$$

where  $\mathbf{a}^* \triangleq \mathbf{h}_d^* + \mathbf{h}_r^* \Phi \mathbf{G}$ ,  $n \sim \mathcal{CN}(0, \sigma^2)$  is additive noise and  $\Phi = \text{diag}(\mathbf{w}) \in \mathbb{C}^{M \times M}$  is the FRIS reflection-selection matrix.

Herein, (5) can be equivalently written as

$$y = \mathbf{h}_d^* \mathbf{f}_B s + \sum_{m=1}^M w_m h_{r,m}^* \mathbf{G}_{m,:} \mathbf{f}_B s + n. \quad (6)$$

For convenience, define the cascaded coefficient

$$h_m \triangleq h_{r,m}^* \mathbf{G}_{m,:} \mathbf{f}_B \quad (m = 1, \dots, M), \quad (7)$$

and define the direct-path scalar  $d \triangleq \mathbf{h}_d^* \mathbf{f}_B$ . Then (6) yields the compact scalar form

$$y = \left( d + \sum_{m=1}^M w_m h_m \right) s + n. \quad (8)$$

Herein, each selected FRIS port  $m$  applies a reflection coefficient  $w_m$  chosen from a finite unit-modulus codebook

$$\mathcal{W}_m \subset \{w \in \mathbb{C} : |w|=1\}, \quad (9)$$

which models discrete phase resolution. Since the zero-coefficient corresponds to unselected port, we define the augmented feasible set for FRIS port  $m$ :

$$\Theta_m \triangleq \{0\} \cup \mathcal{W}_m \quad (m = 1, \dots, M). \quad (10)$$

### B. Problem Formulation

From (8), we define the effective channel coefficient  $z$  as

$$z \triangleq d + \sum_{m=1}^M w_m h_m, \quad (11)$$

whose magnitude represents the resulting beamforming gain at the user. Accordingly, the FRIS configuration problem for the maximization of beamforming gain is formulated as

$$\begin{aligned} & \max_{\{w_m\}, \Gamma, \mathbf{f}_B} \left| d + \sum_{m=1}^M w_m h_m \right| \\ & \text{s.t. } w_m \in \Theta_m \quad (m = 1, \dots, M), \quad \|\mathbf{f}_B\|_2^2 \leq P \\ & \quad \underbrace{|\{m \in \{1, \dots, M\} : w_m \neq 0\}|}_{\triangleq \Gamma} = M_o, \end{aligned} \quad (12)$$

where  $\Gamma \subseteq \{1, \dots, M\}$  denote the selected-port index set with  $|\Gamma| = M_o$ . For a given  $\Gamma$ , set  $w_m = 0$  for all  $m \notin \Gamma$  and optimize  $\{w_m \in \mathcal{W}_m\}_{m \in \Gamma}$ . Then (12) is equivalent to

$$\begin{aligned} & \max_{\{w_m\}, \Gamma, \mathbf{f}_B} \left| d + \sum_{m \in \Gamma} w_m h_m \right| \\ & \text{s.t. } w_m \in \mathcal{W}_m \quad (m \in \Gamma), \quad \|\mathbf{f}_B\|_2 \leq P. \end{aligned} \quad (13)$$

Due to the strong coupling between  $\mathbf{f}_B$ ,  $\{w_m\}$ , and  $\Gamma$  through the effective channel gain, together with the combinatorial nature of choosing  $\Gamma$  from  $\{1, \dots, M\}$ , (13) becomes highly nonconvex, making direct joint optimization intractable. To address this difficulty, we employ an AO framework that decomposes the original problem into two subproblems; beamformer design and FRIS configuration, which are solved in an iterative manner.

### III. PROPOSED APPROACH: UPDATE OF $\mathbf{f}_B$

For fixed  $\{w_m\}$  and  $\Gamma$ , (13) reduces to

$$\max_{\mathbf{f}_B} |\mathbf{a}^* \mathbf{f}_B| \text{ s.t. } \|\mathbf{f}_B\|_2^2 \leq P, \quad (14)$$

whose solution  $\mathbf{f}_B^*$  is trivially given by MRT beamformer:

$$\mathbf{f}_B^* = \sqrt{P} \frac{\mathbf{a}}{\|\mathbf{a}\|_2}. \quad (15)$$

### IV. PROPOSED APPROACH: UPDATE OF $\{w_m\}$ AND $\Gamma$ (GENERAL CASE)

#### A. Transformation to FRIS-Only Subproblem

For fixed  $\mathbf{f}_B$  in (15), plugging it into (12), the original problem is equivalently reduced to

$$\begin{aligned} & \max_{\{w_m\}, \Gamma} \left| d + \sum_{m=1}^M w_m h_m \right| \\ & \text{s.t. } w_m \in \Theta_m \quad (m = 1, \dots, M), \\ & \quad \underbrace{|\{m \in \{1, \dots, M\} : w_m \neq 0\}|}_{\triangleq \Gamma} = M_o. \end{aligned} \quad (16)$$

Define the feasible reflected-sum set with respect to  $\Gamma$  as

$$\mathcal{Z}(\Gamma) \triangleq \sum_{m \in \Gamma} h_m \mathcal{W}_m, \quad (17)$$

which is a Minkowski sum of finite sets. The overall feasible reflected-sum set under  $M_o$ -port selection is the finite union

$$\mathcal{Z}_{M_o} \triangleq \bigcup_{\substack{\Gamma \subseteq \{1, \dots, M\} \\ |\Gamma| = M_o}} \mathcal{Z}(\Gamma). \quad (18)$$

With  $d$ , the overall feasible combined-sum set is the translation

$$\mathcal{Z}_{M_o, t} \triangleq d + \mathcal{Z}_{M_o} = \{d + z : z \in \mathcal{Z}_{M_o}\}. \quad (19)$$

Therefore, (12) can be equivalently rewritten as

$$\max_z |z| \text{ s.t. } z \in \mathcal{Z}_{M_o, t}. \quad (20)$$

#### B. Equivalent Transformations

The proposed method proceeds through the following equivalent transformations:

$$\begin{aligned} & \max_{z \in \mathcal{Z}_{M_o, t}} |z| \stackrel{(a)}{=} \max_{z \in \mathcal{P}_{M_o, t}} |z| \stackrel{(b)}{=} \max_{|u|=1} h_{\mathcal{P}_{M_o, t}}(u) \\ & \stackrel{(c)}{=} \max_{\phi \in [0, 2\pi)} h_{\mathcal{P}_{M_o, t}}(e^{j\phi}), \end{aligned} \quad (21)$$

where  $h_{(.)}$  is a support function will be defined later, and

$$\mathcal{P}_{M_o, t} \triangleq \text{Conv}(\mathcal{Z}_{M_o, t}) = \text{Conv}(d + \mathcal{Z}_{M_o}) = d + \mathcal{P}_{M_o}, \quad (22)$$

where  $\text{Conv}(\cdot)$  is the convex hull of the given set [38], and  $\mathcal{P}_{M_o} \triangleq \text{Conv}(\mathcal{Z}_{M_o})$  [39]. This reduces the original mixed discrete optimization into a one-dimensional search over  $\phi$ .

1) *Equality (a): Convexification Without Loss of Optimality:*

**Lemma 1.** *It holds that*

$$\max_{z \in \mathcal{Z}_{M_o,t}} |z| = \max_{z \in \mathcal{P}_{M_o,t}} |z|. \quad (23)$$

*Proof.* Since  $\mathcal{Z}_{M_o,t}$  is compact by definition, we can use [35, Lemma 1].  $\blacksquare$

Lemma 1 implies that convexifying the feasible reflected-sum set does not alter the optimal beamforming gain, i.e., the maximum achievable magnitude is always attained on the boundary of the convex hull, allowing the original discrete and nonconvex optimization over  $\mathcal{Z}_{M_o,t}$  to be equivalently solved over its convex hull  $\mathcal{P}_{M_o,t}$  without any loss of optimality.

2) *Equality (b)-(c): Norm Maximization via Support Functions:* We first recall the following trivial identity.

**Lemma 2.** *For any  $z \in \mathbb{C}$ , it holds that*

$$|z| = \max_{|u|=1} \Re\{u^* z\}. \quad (24)$$

Moreover, if  $z \neq 0$ , the maximizers are  $u^* = e^{j \arg(z)}$ .

*Proof.* Write  $z = |z|e^{j\theta}$  and set  $u = e^{j\phi}$ . Then  $\Re\{u^* z\} = |z|\cos(\theta - \phi) \leq |z|$ , with equality iff  $\phi = \theta \pmod{2\pi}$ , which leads to  $u^* = e^{j \arg(z)}$ .  $\blacksquare$

For any nonempty compact convex set  $\mathcal{C} \subset \mathbb{C}$ , define its support function as

$$h_{\mathcal{C}}(u) \triangleq \max_{z \in \mathcal{C}} \Re\{u^* z\} \quad (|u|=1). \quad (25)$$

Applying Lemma 2 and the definition above to  $\mathcal{C} = \mathcal{P}_{M_o,t}$ :

$$\begin{aligned} \max_{z \in \mathcal{P}_{M_o,t}} |z| &= \max_{z \in \mathcal{P}_{M_o,t}} \max_{|u|=1} \Re\{u^* z\} \\ &= \max_{|u|=1} \max_{z \in \mathcal{P}_{M_o,t}} \Re\{u^* z\} \\ &= \max_{|u|=1} h_{\mathcal{P}_{M_o,t}}(u) \\ &= \max_{\phi \in [0, 2\pi)} h_{\mathcal{P}_{M_o,t}}(e^{j\phi}). \end{aligned} \quad (26)$$

Combining Lemma 1 with (26) establishes (21). Hence, it remains to evaluate  $h_{\mathcal{P}_{M_o,t}}(e^{j\phi})$  efficiently for given  $\phi$ .

The geometry in Fig. 2 illustrates the interpretation of  $h_{\mathcal{C}}(u)$ . For a general  $\mathcal{C} \subset \mathbb{C}$  in Fig. 2a,  $h_{\mathcal{C}}(u)$  represents the maximum projection of  $\mathcal{C}$  onto the direction  $u = e^{j\phi}$ , obtained by translating a line orthogonal to  $u$  until it first touches the boundary of  $\mathcal{C}$ . As  $\phi$  varies, the supporting point moves continuously along the boundary. By contrast, when  $\mathcal{C}$  is a polygon induced by a finite phase codebook in Fig. 2b, the maximizer is always attained at a vertex [38], [39]. Consequently,  $h_{\mathcal{C}}(u)$  becomes piecewise linear in  $\phi$ , with the maximizing vertex remaining unchanged over angular intervals and switching at the bisectors between adjacent vertices, leading to a direction-dependent vertex selection. This observation enables an algorithmic realization for general and regular  $M_p$ -gon codebooks in Section IV-D and V, respectively, where the optimal vertex, interpretable as the one whose associated Thales circle dominates the projection along a given direction [35], and hence the optimal quantized phase, can

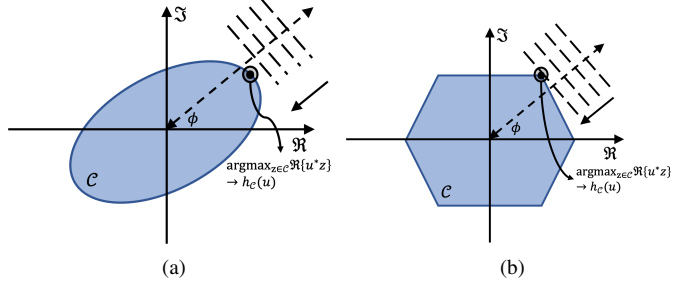


Fig. 2. Geometrical illustration of  $h_{\mathcal{C}}(u)$  with respect to (a) general and (b) polygon type of  $\mathcal{C}$ .

be efficiently identified through direction-dependent interval partitioning.

### C. Evaluation of $h_{\mathcal{P}_{M_o,t}}(e^{j\phi})$

1) *Support-Function Identities and Translation Decomposition:* We use the following standard identities of support functions. Throughout, all sets are assumed to be nonempty and compact; whenever Minkowski-sum additivity is invoked, the involved sets are convex [39]:

$$\begin{aligned} h_{\text{Conv}(\mathcal{S})}(u) &= \max_{z \in \mathcal{S}} \Re\{u^* z\}, \\ h_{\text{Conv}(\cup_i \mathcal{C}_i)}(u) &= \max_i h_{\mathcal{C}_i}(u), \\ h_{\mathcal{C}_1 + \mathcal{C}_2}(u) &= h_{\mathcal{C}_1}(u) + h_{\mathcal{C}_2}(u). \end{aligned} \quad (27)$$

By (22), the support function decomposes as

$$h_{\mathcal{P}_{M_o,t}}(u) = h_{\{d\}}(u) + h_{\mathcal{P}_{M_o}}(u) = \Re\{u^* d\} + h_{\mathcal{P}_{M_o}}(u), \quad (28)$$

and setting  $u = e^{j\phi}$  yields

$$h_{\mathcal{P}_{M_o,t}}(e^{j\phi}) = \Re\{e^{-j\phi} d\} + h_{\mathcal{P}_{M_o}}(e^{j\phi}). \quad (29)$$

Note that the direct link contributes an additive directional term that depends only on  $\phi$  and does not couple across ports.

2) *Support Function of  $\mathcal{P}_{M_o,t}$  and Portwise Scores:* As in the reflected-only case, applying (27) to  $\mathcal{P}_{M_o} = \text{Conv}(\mathcal{Z}_{M_o})$  yields, for any  $|u|=1$ ,

$$h_{\mathcal{P}_{M_o}}(u) = \max_{\substack{\Gamma \subseteq \{1, \dots, M\} \\ |\Gamma|=M_o}} \sum_{m \in \Gamma} h_{h_m \text{Conv}(\mathcal{W}_m)}(u). \quad (30)$$

Let  $u = e^{j\phi}$  with  $\phi \in [0, 2\pi)$ . Define the port-wise score

$$\begin{aligned} s_m(\phi) &\triangleq h_{h_m \text{Conv}(\mathcal{W}_m)}(e^{j\phi}) \\ &= \max_{w \in \mathcal{W}_m} \Re\{e^{-j\phi} h_m w\} \quad (m = 1, \dots, M), \end{aligned} \quad (31)$$

which leads to

$$h_{\mathcal{P}_{M_o}}(e^{j\phi}) = \max_{\substack{\Gamma \subseteq \{1, \dots, M\} \\ |\Gamma|=M_o}} \sum_{m \in \Gamma} s_m(\phi). \quad (32)$$

Combining (29) and (32) yields

$$h_{\mathcal{P}_{M_o,t}}(e^{j\phi}) = \Re\{e^{-j\phi} d\} + \max_{\substack{\Gamma \subseteq \{1, \dots, M\} \\ |\Gamma|=M_o}} \sum_{m \in \Gamma} s_m(\phi). \quad (33)$$

#### D. Top- $M_o$ Induced FRIS Port Selection

Since the second term in (33) is a linear sum of per-port scores under a cardinality constraint, an optimizer is obtained by selecting the  $M_o$  largest scores:

$$\Gamma^*(\phi) \in \arg \max_{\substack{\Gamma \subseteq \{1, \dots, M\} \\ |\Gamma|=M_o}} \sum_{m \in \Gamma} s_m(\phi) = \text{Top-}M_o(\{s_m(\phi)\}_{m=1}^M), \quad (34)$$

where ties may be broken arbitrarily. Note that  $\Re\{e^{-j\phi}d\}$  does not affect this selection rule because it is independent of  $\Gamma$ . Given  $\Gamma^*(\phi)$ , for each selected port choose

$$\hat{w}_m(\phi) \in \arg \max_{w \in \mathcal{W}_m} \Re\{e^{-j\phi}h_m w\} \quad (m \in \Gamma^*(\phi)), \quad (35)$$

and set  $w_m = 0$  for  $m \notin \Gamma^*(\phi)$ . This construction attains  $h_{\mathcal{P}_{M_o}}(e^{j\phi})$  in (32).

Herein, we provide a geometric interpretation of the proposed FRIS port selection algorithm, illustrated by Fig. 3, by viewing  $s_m(\phi)$  as a directional projection over  $h_m \text{Conv}(\mathcal{W}_m)$ . Herein, each  $h_m w$  ( $w \in \mathcal{W}_m$ ) induces a Thales circle  $e^{j\theta} \Re\{e^{-j\theta}h_m w\}$  ( $\theta \in [0, 2\pi)$ ) with diameter  $[0, h_m w]$ , whose projection along  $e^{j\phi}$  for a given  $\phi$  is  $\Re\{e^{-j\phi}h_m w\}$  [35]. As  $\phi$  varies, each vertex dominates a specific angular interval corresponding to an outer arc of its associated circle, as depicted in the lower part of Fig. 3. Accordingly,  $s_m(\phi)$  is determined by the vertex whose arc contains  $\phi$ , i.e., the one that yields the largest projection in the direction  $e^{j\phi}$ , which coincides with the interpretation in Fig. 2b. This geometric optimization is carried out independently for each  $m$ . The subsequent Top- $M_o$  operation, which yields  $\Gamma^*(\phi)$ , then selects the  $M_o$  ports with the largest individually optimized  $s_m(\phi)$ .

Therefore, the optimal FRIS configuration is obtained by the one-dimensional search with respect to  $\phi$ :

$$\phi^* \in \arg \max_{\phi \in [0, 2\pi)} \left( \underbrace{\Re\{e^{-j\phi}d\} + \sum_{m \in \Gamma^*(\phi)} s_m(\phi)}_{=h_{\mathcal{P}_{M_o,t}}(e^{j\phi})} \right) \quad (36)$$

and the corresponding final FRIS coefficients are

$$w_m^* = \begin{cases} \hat{w}_m(\phi^*) & (m \in \Gamma^*(\phi^*)), \\ 0 & (\text{otherwise}). \end{cases} \quad (37)$$

The achieved combined sum is

$$z^* = d + \sum_{m \in \Gamma^*(\phi^*)} h_m \hat{w}_m(\phi^*), \quad (38)$$

and  $|z^*|$  equals the optimal value of (12). The overall FRIS configuration procedure is summarized in Algorithm 1.

#### V. PROPOSED APPROACH: UPDATE OF $\{w_m\}$ AND $\Gamma$ (REGULAR $M_p$ -GON CODEBOOK)

In this section, we specialize the proposed framework in Section IV to the practically important case where each feasible reflection set is a uniform  $M_p$ -ary phase-shifter

---

#### Algorithm 1 Proposed FRIS Configuration Algorithm

---

**Require:**  $\{h_m\}_{m=1}^M$ ,  $\{\mathcal{W}_m\}_{m=1}^M$ ,  $M_o$ ,  $d$

- 1: Partition  $[0, 2\pi)$  into finitely many intervals and pick one representative  $\bar{\phi}$  per interval.
- 2: **for** each representative  $\bar{\phi}$  **do**
- 3:   **for**  $m = 1$  to  $M$  **do**
- 4:     Compute  $s_m(\bar{\phi})$  using (31) (or (45) for the regular  $M_p$ -gon case) by determining  $w \in \mathcal{W}_m$  according to the procedure illustrated in Fig. 3.
- 5:   **end for**
- 6:   Determine  $\Gamma^*(\bar{\phi})$  via (34).
- 7:   Evaluate  $\hat{w}_m(\bar{\phi})$  ( $m \in \Gamma^*(\bar{\phi})$ ) by (35).
- 8:   Evaluate  $h_{\mathcal{P}_{M_o,t}}(e^{j\bar{\phi}})$  by (36).
- 9: **end for**
- 10: Choose  $\phi^*$  by (36).
- 11: Set  $w_m^*$  by (37) and compute  $z^*$  by (38).
- 12: **return**  $\Gamma^*(\phi^*)$ ,  $\{w_m^*\}$ , and  $z^*$

---

codebook [27], [28], namely the vertices of a regular  $M_p$ -gon on the unit circle. This specialization yields (i) closed-form expressions for  $s_m(\phi)$  and the corresponding optimal codeword, and (ii) a finite set of critical angles that avoids exhaustive angular sweeping.

#### A. Regular $M_p$ -gon Codebook and Quantization Residual

Assume that all ports share the same  $M_p$ -ary phase-shifter codebook

$$\mathcal{W}_m = \mathcal{W}_{M_p} \triangleq \left\{ e^{j \frac{2\pi k}{M_p}} \right\}_{k=0}^{M_p-1} \quad (\forall m), \quad (39)$$

where  $M_p \geq 2$  denotes the phase resolution. We then use the principal-value mapping  $\text{wrap} : \mathbb{R} \rightarrow (-\pi, \pi]$  defined by

$$\text{wrap}(\phi) \triangleq \phi - 2\pi \left\lfloor \frac{\phi + \pi}{2\pi} \right\rfloor, \quad (40)$$

which maps  $\phi$  to its unique equivalent in the principal interval  $(-\pi, \pi]$ , and define the phase-quantization residual

$$\delta_{M_p}(\phi) \triangleq \min_{k \in \{0, \dots, M_p-1\}} \left| \text{wrap}\left(\phi - \frac{2\pi k}{M_p}\right) \right| \in \left[ 0, \frac{\pi}{M_p} \right], \quad (41)$$

which quantifies the minimum angular mismatch between  $\phi$  and the nearest phase point in the  $M_p$ -ary quantized codebook.

Thereafter, the support function of the  $M_p$ -gon can be characterized by the following theorem:

**Theorem 3.** For any  $\phi \in \mathbb{R}$ ,

$$h_{\text{Conv}(\mathcal{W}_{M_p})}(e^{j\phi}) = \max_{w \in \mathcal{W}_{M_p}} \Re\{e^{-j\phi}w\} = \cos(\delta_{M_p}(\phi)). \quad (42)$$

Moreover, a maximizer is given by any

$$\begin{aligned} \hat{w}_m(\phi) &= e^{j \frac{2\pi}{M_p} k_m^*(\phi)}, \\ k_m^*(\phi) &\in \arg \min_{k \in \{0, \dots, M_p-1\}} \left| \text{wrap}\left(\phi - \frac{2\pi k}{M_p}\right) \right|. \end{aligned} \quad (43)$$

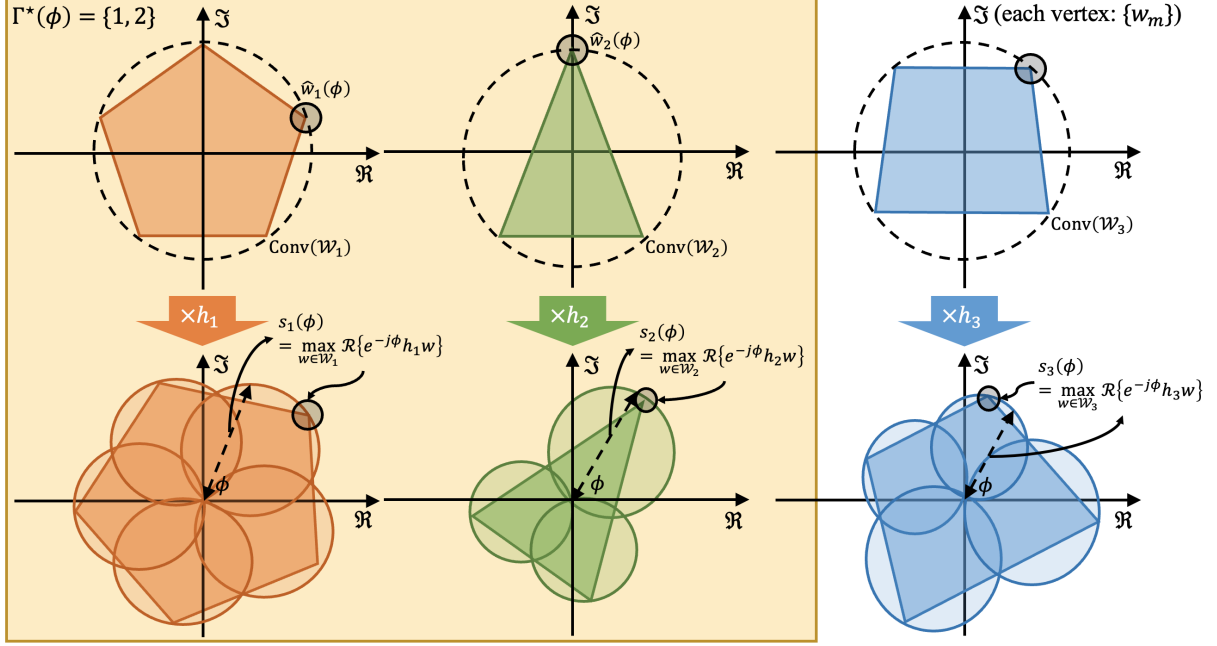


Fig. 3. Geometric illustration and the resulting Top- $M_o$  port selection based on arc dominance in the Thales-circle representation with  $M = 3$  and  $M_0 = 2$ .

*Proof.* Since  $\text{Conv}(\mathcal{W}_{M_p})$  is the convex hull of finitely many points, its support function is attained at a vertex:

$$\begin{aligned} h_{\text{Conv}(\mathcal{W}_{M_p})}(e^{j\phi}) &= \max_k \Re\{e^{-j\phi} e^{j\frac{2\pi k}{M_p}}\} \\ &= \max_k \cos\left(\phi - \frac{2\pi k}{M_p}\right). \end{aligned} \quad (44)$$

The maximizing  $k$  is the nearest phase grid point (in principal value), which yields  $\delta_{M_p}(\phi)$  in (41), proving (42). The maximizer characterization follows directly, giving (43). ■

### B. Port and Direct-Term Score, and Optimal Codeword

Let  $\alpha_m \triangleq \arg(h_m)$  and  $a_m \triangleq |h_m|$  for all  $m$  and let  $\alpha_d \triangleq \arg(d)$  and  $a_d \triangleq |d|$ . Then  $s_m(\phi)$  and the directional term admit the following closed-form:

**Corollary 3.1.** Under (39), for any  $\phi \in [0, 2\pi)$ ,

$$s_m(\phi) = a_m \cos\left(\delta_{M_p}(\phi - \alpha_m)\right) \quad (m = 1, \dots, M). \quad (45)$$

Moreover,

$$\Re\{e^{-j\phi} d\} = a_d \cos(\phi - \alpha_d). \quad (46)$$

An optimal FRIS codeword can be chosen as

$$\begin{aligned} \hat{w}_m(\phi - \alpha_m) &= e^{j\frac{2\pi}{M_p} k_m^*(\phi - \alpha_m)}, \\ k_m^*(\phi - \alpha_m) &\in \arg \min_k \left| \text{wrap}\left(\phi - \alpha_m - \frac{2\pi k}{M_p}\right) \right|. \end{aligned} \quad (47)$$

*Proof.* By definition,

$$\begin{aligned} s_m(\phi) &= \max_{w \in \mathcal{W}_{M_p}} \Re\{e^{-j\phi} h_m w\} \\ &= \max_{w \in \mathcal{W}_{M_p}} \Re\{e^{-j(\phi - \alpha_m)} a_m w\} \\ &= a_m \max_{w \in \mathcal{W}_{M_p}} \Re\{e^{-j(\phi - \alpha_m)} w\}. \end{aligned} \quad (48)$$

Applying Theorem 3 with  $\phi \leftarrow \phi - \alpha_m$  yields (45), and the maximizer follows from (43), proving (47). The direct-term identity follows from  $d = a_d e^{j\alpha_d}$  and  $\Re\{e^{-j\phi} d\} = a_d \cos(\phi - \alpha_d)$ , proving (46). ■

The geometrical illustration of deriving  $h_{\text{Conv}(\mathcal{W}_{M_p})}(e^{j\phi})$  and  $s_m(\phi)$  is given in Fig. 4. Herein, the support function is interpreted as the maximum projection of the convex hull of the discrete phase codebook onto the direction  $e^{j\phi}$ , which is attained at the codeword whose phase is closest to  $\phi$ , leading to the cosine form governed by  $\delta_{M_p}(\cdot)$ . When incorporating  $h_m$ , this convex set undergoes a rotation by  $\alpha_m$  and a scaling by  $a_m$ , so that the resulting  $s_m(\phi)$  naturally captures both channel magnitude and phase quantization effects in a unified geometric manner.

With Corollary 3.1,  $s_m(\phi)$  and  $\hat{w}_m(\phi - \alpha_m)$  are available for  $\phi \in [0, 2\pi)$ , and the objective in (36) becomes

$$h_{\mathcal{P}_{M_o,t}}(e^{j\phi}) = a_d \cos(\phi - \alpha_d) + \sum_{m \in \Gamma^*(\phi)} a_m \cos\left(\delta_{M_p}(\phi - \alpha_m)\right), \quad (49)$$

where  $\Gamma^*(\phi) = \text{Top-}M_o(\{s_m(\phi)\})$ . Thus, for each  $\phi$ , we can evaluate  $h_{\mathcal{P}_{M_o,t}}(e^{j\phi})$  with  $\Gamma^*(\phi)$  and  $\hat{w}_m(\phi - \alpha_m)$  ( $m \in \Gamma^*(\phi)$ ) by (47), and assigning  $\phi^*$  and  $w_m^*$  as in (36) and (37), respectively.

### C. Maximization of $h_{\mathcal{P}_{M_o,t}}(e^{j\phi})$ via a Finite Candidate Set

For evaluation of  $h_{\mathcal{P}_{M_o,t}}(e^{j\phi})$  in (49), although it is a sum of cosine-type terms, the dependence of (i)  $k_m^*(\phi - \alpha_m)$  embedded in  $\delta_{M_p}$  and (ii)  $\Gamma^*(\phi)$  on  $\phi$  makes  $h_{\mathcal{P}_{M_o,t}}(e^{j\phi})$  piecewise smooth with finitely many nondifferentiable points. In this subsection, we show that the global maximizer can be obtained by checking only a finite set of candidate angles, thereby avoiding generic one-dimensional search.

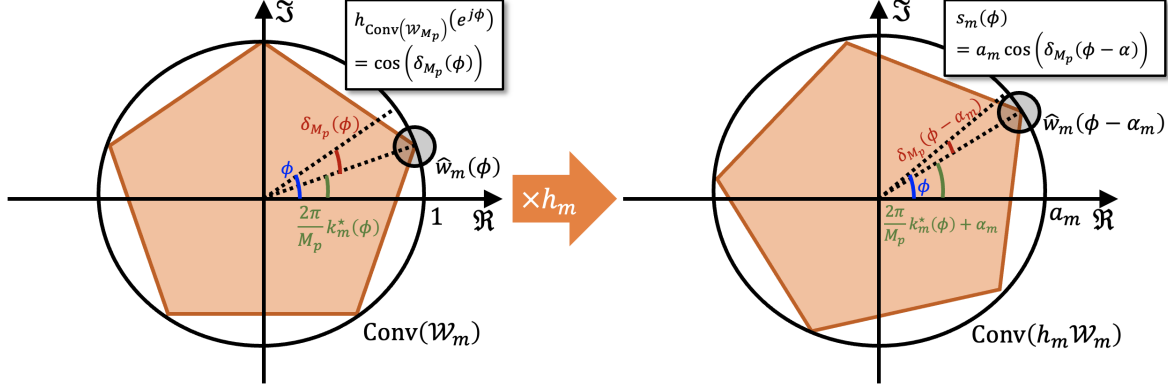


Fig. 4. Geometric interpretation of  $h_{\text{Conv}(\mathcal{W}_{M_p})}(e^{j\phi})$  and  $s_m(\phi)$  for a regular  $M_p$ -gon phase codebook and the resulting per-port score with  $M_p = 5$ . The left figure depicts  $\text{Conv}(\mathcal{W}_{M_p})$  of the unit-modulus  $M_p$ -ary phase-shifter codebook and the evaluation of  $h_{\text{Conv}(\mathcal{W}_{M_p})}(e^{j\phi}) = \cos(\delta_{M_p}(\phi))$  along direction  $e^{j\phi}$ , while the right figure illustrates the scaled and rotated convex set  $\text{Conv}(h_m \mathcal{W}_{M_p})$ , where multiplication by  $h_m = a_m e^{j\alpha_m}$  induces a rotation by  $\alpha_m$  and a radial scaling by  $a_m$ , resulting in  $s_m(\phi) = a_m \cos(\delta_{M_p}(\phi - \alpha_m))$ .

1) *Quantization-Induced Linearization*: For fix  $m$ , over any interval  $\mathcal{I}$  where  $k_m^*(\phi - \alpha_m)$  stays constant, say  $k_m^*(\phi - \alpha_m) \equiv k_m$ , we have

$$\cos(\delta_{M_p}(\phi - \alpha_m)) = \cos\left(\phi - \alpha_m - \frac{2\pi k_m}{M_p}\right) (\phi \in \mathcal{I}), \quad (50)$$

because the principal-value difference to the nearest grid point is simply the signed offset inside that cell. Accordingly, on such an  $\mathcal{I}$ , each per-port term becomes an ordinary cosine with a fixed phase shift. The  $k_m$ -switching (boundary) angles for port  $m$  occur when  $\phi - \alpha_m$  lies on the midpoints between adjacent grid points, which correspond to the midpoints of the vertices of given regular  $M_p$ -gon:

$$\Phi_m^q \triangleq \left\{ \alpha_m + \frac{2\pi k}{M_p} \pm \frac{\pi}{M_p} \pmod{2\pi} : k = 0, \dots, M_p - 1 \right\}. \quad (51)$$

Let  $\Phi^q \triangleq \bigcup_{m=1}^M \Phi_m^q$  denote the global set of quantization breakpoints.

2) *Top- $M_o$  Switching and Score-Crossing Angles*: Even if the quantizer indices are fixed,  $\Gamma^*(\phi)$  can switch when the ordering of  $\{s_m(\phi)\}$  changes. A switch can only happen at  $\phi$  where two scores tie:

$$s_m(\phi) = s_n(\phi) \quad (m \neq n). \quad (52)$$

Since each  $s_m(\phi)$  is piecewise cosine by (50), within any region where all involved  $k_m^*(\phi - \alpha_m)$  and  $k_n^*(\phi - \alpha_n)$  are fixed, (52) reduces to

$$a_m \cos(\phi - \beta_m) = a_n \cos(\phi - \beta_n), \quad (53)$$

with  $\beta_i \triangleq \alpha_i + \frac{2\pi k_i}{M_p}$  ( $i = m, n$ ) fixed. Equation (53) is equivalent to a linear constraint in  $\cos \phi$  and  $\sin \phi$ :

$$\begin{aligned} & (a_m \cos \beta_m - a_n \cos \beta_n) \cos \phi \\ & + (a_m \sin \beta_m - a_n \sin \beta_n) \sin \phi = 0, \end{aligned} \quad (54)$$

whose solutions (if any) consist of at most two angles in  $[0, 2\pi]$ . Collect all such score-crossing angles over all pairs  $(m, n)$  ( $m \neq n$ ) into a finite set  $\Phi^{\text{top}}$ , which correspond to

points at which the relative ordering between  $s_m(\phi)$  and  $s_n(\phi)$  changes and may therefore alter  $\Gamma^*(\phi)$ .

3) *Piecewise Sinusoid Structure and A Finite Maximizer Test*: Define the global breakpoint set

$$\Phi_{\text{br}} \triangleq \Phi^q \cup \Phi^{\text{top}}, \quad (55)$$

and sort them over  $[0, 2\pi]$  to obtain a partition into finitely many open intervals  $\mathcal{I}_\ell \triangleq (\varphi_\ell, \varphi_{\ell+1})$  and each interval contains no breakpoint.

**Lemma 4.** *On  $\mathcal{I}_\ell$ , all  $\{k_m^*(\phi - \alpha_m)\}_{m=1}^M$  and  $\Gamma^*(\phi)$  remain constant.*

*Proof.* By construction,  $\mathcal{I}_\ell$  contains no quantization breakpoint, so each  $k_m^*(\phi - \alpha_m)$  cannot change inside  $\mathcal{I}_\ell$ , establishing index constancy. Likewise,  $\mathcal{I}_\ell$  contains no score-tie point, so the ordering of  $\{s_m(\phi)\}$  cannot change, and hence  $\Gamma^*(\phi) = \text{Top-}M_o(\{s_m(\phi)\})$  remains constant. ■

On a fixed  $\mathcal{I}_\ell$ , denote the constant active set by  $\Gamma_\ell$  and the constant quantized phases by  $\beta_{m,\ell} \triangleq \alpha_m + \frac{2\pi k_{m,\ell}}{M_p}$  ( $m \in \Gamma_\ell$ ). Then, by (50), the objective on  $\mathcal{I}_\ell$  becomes a single sinusoid plus a constant:

$$\begin{aligned} h_{\mathcal{P}_{M_o,\ell}}(e^{j\phi}) &= a_d \cos(\phi - \alpha_d) + \sum_{m \in \Gamma_\ell} a_m \cos(\phi - \beta_{m,\ell}) \\ &= \Re \left\{ e^{-j\phi} \left( d + \sum_{m \in \Gamma_\ell} a_m e^{j\beta_{m,\ell}} \right) \right\} \\ &= \Re \left\{ e^{-j\phi} C_\ell \right\} (\phi \in \mathcal{I}_\ell), \end{aligned} \quad (56)$$

where we define the region-wise complex resultant

$$C_\ell \triangleq d + \sum_{m \in \Gamma_\ell} a_m e^{j\beta_{m,\ell}} = |C_\ell| e^{j\angle C_\ell}. \quad (57)$$

**Lemma 5.** *On  $\mathcal{I}_\ell$ , the maximizer of (56) is attained either (i) at the interior stationary point  $\phi = \angle C_\ell$  if  $\angle C_\ell \in \mathcal{I}_\ell$ , or (ii) at an endpoint  $\varphi_\ell$  or  $\varphi_{\ell+1}$ .*

*Proof.* From (56),  $h(\phi) = |C_\ell| \cos(\phi - \angle C_\ell)$  on  $\mathcal{I}_\ell$ . The function is smooth and unimodal between consecutive extrema,

---

**Algorithm 2** Maximizing  $h_{\mathcal{P}_{M_o,t}}(e^{j\phi})$  for a Regular  $M_p$ -gon

---

**Require:**  $\{a_m, \alpha_m\}_{m=1}^M, a_d, \alpha_d, M_o, M_p$ 
1: Construct  $\Phi^q = \bigcup_{m=1}^M \Phi_m^q$  by (51).2: Initialize  $\Phi^{\text{top}} \leftarrow \emptyset$ .3: Sort  $\Phi^q$  and form  $\{\mathcal{I}_\ell\}_\ell$ .4: **for** each interval  $\mathcal{I}_\ell$  **do**5:   Pick any  $\bar{\phi} \in \mathcal{I}_\ell$ .6:   Compute  $s_m(\bar{\phi}) = a_m \cos(\delta_{M_p}(\bar{\phi} - \alpha_m))$  ( $\forall m$ ).7:   Determine  $\Gamma_\ell = \text{Top-}M_o(\{s_m(\bar{\phi})\})$ .8:   Detect changes in the ordering of  $\{s_m(\bar{\phi})\}$  by examining (52) that occur at the boundaries of  $\mathcal{I}_\ell$ .9:   Append the corresponding angles into  $\Phi^{\text{top}}$ .10: Compute  $C_\ell$  by (57).11: **end for**12: Set  $\Phi_{\text{cand}} \leftarrow \Phi^q \cup \Phi^{\text{top}} \cup \{\angle C_\ell \in \mathcal{I}_\ell\}$ .13: Evaluate  $h_{\mathcal{P}_{M_o,t}}(e^{j\phi})$  at all  $\phi \in \Phi_{\text{cand}}$  using (49).14: Output  $\phi^* \in \arg \max_{\phi \in \Phi_{\text{cand}}} h_{\mathcal{P}_{M_o,t}}(e^{j\phi})$ .15: **return**  $\phi^*$ 


---

and its only stationary point in a  $2\pi$ -period is at  $\phi = \angle C_\ell$  (mod  $2\pi$ ). Therefore, the maximum over an open interval is attained at the stationary point if it lies inside; otherwise it is attained at the boundary of the interval.  $\blacksquare$

**Theorem 6.** Define the finite candidate set

$$\Phi_{\text{cand}} \triangleq \Phi_{\text{br}} \cup \{\angle C_\ell : \angle C_\ell \in \mathcal{I}_\ell\}. \quad (58)$$

Then the global maximizer of  $h_{\mathcal{P}_{M_o,t}}(e^{j\phi})$  over  $\phi \in [0, 2\pi)$  satisfies

$$\phi^* \in \arg \max_{\phi \in [0, 2\pi)} h_{\mathcal{P}_{M_o,t}}(e^{j\phi}) \subseteq \arg \max_{\phi \in \Phi_{\text{cand}}} h_{\mathcal{P}_{M_o,t}}(e^{j\phi}). \quad (59)$$

*Proof.* By Lemma 4, on each  $\mathcal{I}_\ell$  the objective has the sinusoidal form (56). By Lemma 5, the maximum over  $\mathcal{I}_\ell$  is achieved either at  $\angle C_\ell$  or at an endpoint, and every endpoint belongs to  $\Phi_{\text{br}}$ . Hence, the maximum over each region is attained at some point in  $\Phi_{\text{cand}}$ . Taking the maximum over all regions yields (59).  $\blacksquare$

Theorem 6 reduces the continuous maximization of  $h_{\mathcal{P}_{M_o,t}}(e^{j\phi})$  to evaluating finitely many candidates. A practical procedure is summarized in Algorithm 2.

*Remark 1.* In implementation of finding  $\Phi^{\text{top}}$ , it is not necessary to explicitly solve all pairwise crossing equations. Instead, we construct  $\Phi^{\text{top}}$  by inspecting only the boundaries of  $\{\mathcal{I}_\ell\}$  and detecting neighboring score ties that induce a local change in the Top- $M_o$  ordering. This is sufficient because within each  $\mathcal{I}_\ell$  all score functions are smooth and their relative ordering remains invariant, so that any ordering change must occur at an interval boundary.

## VI. PROPOSED AO FRAMEWORK

Based on the results, we develop an AO framework to solve (12). The proposed AO alternates between (A) an update of  $\mathbf{f}_B$  and (B) an optimal FRIS update. Starting from an initial feasible  $\mathbf{w}^{(0)}$  and with iteration  $t$ , the AO iterates between the following two subproblems.

---

**Algorithm 3** Proposed AO Framework

---

**Require:**  $\mathbf{h}_d, \mathbf{h}_r, \mathbf{G}, \{\mathcal{W}_m\}_{m=1}^M, M_o, P, \epsilon$ 
1: Initialize  $\mathbf{w}^{(0)}$  with  $|\{m : w_m^{(0)} \neq 0\}| = M_o$ ; set  $t = 0$ .2: **repeat**3:   Set  $\mathbf{f}_B^{(t+1)}$  by (60).4:   Compute  $d^{(t+1)}$  and  $\{h_m^{(t+1)}\}$  by (62).5:   Solve (61) to obtain  $(\Gamma^{(t+1)}, \mathbf{w}^{(t+1)})$  and the corresponding  $t$ th objective value  $|z^{*(t+1)}|$  ( $z^{(0)} = 0$ ).6:    $t \leftarrow t + 1$ .7: **until**  $||z^{*(t)}| - |z^{*(t-1)}|| \leq \epsilon$ 8: **return**  $\mathbf{f}_B^{(t)}, \Gamma^{(t)}, \mathbf{w}^{(t)}$ 


---

### A. Update of $\mathbf{f}_B$

For a fixed  $\mathbf{w}^{(t)}$ , the update of  $\mathbf{f}_B$  is by (15) given by

$$\mathbf{f}_B^{(t+1)} = \sqrt{P} \frac{\mathbf{a}(\mathbf{w}^{(t)})}{\|\mathbf{a}(\mathbf{w}^{(t)})\|_2}. \quad (60)$$

### B. Update of $\mathbf{w}$ and $\Gamma$

For a fixed  $\mathbf{f}_B^{(t+1)}$ , we can solve the following FRIS subproblem:

$$\max_{\{w_m\}, \Gamma} \left| d^{(t+1)} + \sum_{m \in \Gamma} h_m^{(t+1)} w_m \right| \quad (61)$$

s.t.  $w_m \in \mathcal{W}_m$  ( $m \in \Gamma$ ),  $|\Gamma| = M_o$ ,

where

$$d^{(t+1)} \triangleq \mathbf{h}_d^* \mathbf{f}_B^{(t+1)}, \quad h_m^{(t+1)} \triangleq h_{r,m}^* \mathbf{G}_{m,:} \mathbf{f}_B^{(t+1)} \quad (\forall m). \quad (62)$$

We apply the proposed framework in Section IV to obtain an update  $(\Gamma^{(t+1)}, \mathbf{w}^{(t+1)})$ . The resulting AO procedure is summarized in Algorithm 3. Since Section VI-A globally maximizes the objective over  $\mathbf{f}_B$  for fixed  $\mathbf{w}^{(t)}$ , and VI-B optimizes the objective over  $(\mathbf{w}, \Gamma)$  for fixed  $\mathbf{f}_B^{(t+1)}$ , the objective sequence is nondecreasing and upper-bounded by system framework (i.e.,  $|z| \leq |d| + \sum_{m \in \Gamma} |h_m|$ ), and thus converges.

## VII. COMPUTATIONAL COMPLEXITY

We analyze the computational complexity of the proposed AO framework by examining the per-iteration cost of each update step. In each AO iteration, the update of  $\mathbf{f}_B$  is performed via the closed-form MRT solution in (60). This step requires computing  $\mathbf{a}$  and its Euclidean norm, which involves matrix-vector multiplications of size  $M \times N$  and therefore incurs a complexity of  $\mathcal{O}(MN)$ . Subsequently, the computation of  $d = \mathbf{h}_d^* \mathbf{f}_B$  and  $\{h_m = h_{r,m}^* \mathbf{G}_{m,:} \mathbf{f}_B\}_{m=1}^M$  also requires  $\mathcal{O}(MN)$  operations, which is of the same order as the beamformer update and thus does not change the overall per-iteration scaling.

1) *Complexity Implication for General Codebooks:* The dominant complexity in each AO iteration arises from the FRIS configuration update. Specifically, the proposed Minkowski-geometry-based algorithm evaluates  $h_{\mathcal{P}_{M_o,t}}(e^{j\phi})$  over  $N_\phi$  candidate directions. For each  $\phi$ ,  $\{s_m(\phi)\}_{m=1}^M$  are computed. In the general finite-codebook case, evaluating each  $s_m(\phi)$  requires  $\mathcal{O}(|\mathcal{W}_m|)$  operations, leading to a total cost of

TABLE II  
SIMULATION PARAMETERS

Parameter	Value
Number of BS antennas $N$	16
Number of FRIS elements $M$ (unless referred)	64 ( $8 \times 8$ )
Number of selected FRIS elements $M_o$	8
Transmit SNR $\frac{P}{\sigma^2}$	0 dB
Carrier frequency	3.5 GHz
Path-loss exponent	2.5
Rician $K$ -factor of $\mathbf{G}$	3 dB
Resolution of phase codebook $ \mathcal{W}_m $ or $M_p$ (unless referred)	8
Normalized FRIS aperture $\bar{W}_x$ (unless referred)	2

$\mathcal{O}\left(\sum_{m=1}^M |\mathcal{W}_m|\right)$  for score computation. The subsequent Top- $M_o$  port selection can be carried out in  $\mathcal{O}(M)$  using selection algorithms, while the optimal codeword assignment for the selected ports can be stored during the score evaluation without additional asymptotic cost. Therefore, the per-direction complexity of the FRIS update is  $\mathcal{O}\left(\sum_{m=1}^M |\mathcal{W}_m| + M\right)$ , and the total FRIS-update complexity per AO iteration scales as  $\mathcal{O}\left(N_\phi \left(\sum_{m=1}^M |\mathcal{W}_m| + M\right)\right)$ . Combining the above steps, the overall computational complexity after  $T$  AO iterations is given by

$$\mathcal{O}\left(T \left(MN + N_\phi \left(\sum_{m=1}^M |\mathcal{W}_m| + M\right)\right)\right). \quad (63)$$

### 2) Complexity Implication for Regular $M_p$ -gon Codebooks:

In the practically case of a regular  $M_p$ -gon codebook, as a function of  $\phi$ ,  $s_m(\phi)$  is piecewise cosine, where its maximizing codeword changes at (51) with at most  $2M_p$  breakpoint angles over  $[0, 2\pi]$ , and the total number of breakpoints across all  $M$  ports scales as  $N_\phi = \mathcal{O}(MM_p)$ . Between any two consecutive breakpoints, the active codeword for each port remains unchanged, and hence  $h_{\mathcal{P}_{M_o,t}}(e^{j\phi})$  is smooth within each interval. As a result, the FRIS-update can be carried out by evaluating  $h_{\mathcal{P}_{M_o,t}}(e^{j\phi})$  at one representative point per interval, leading to a per-iteration complexity of  $\mathcal{O}(N_\phi M)$ . Accordingly, the overall AO complexity simplifies to

$$\mathcal{O}\left(T(MN + M^2M_p)\right). \quad (64)$$

As demonstrated in Section VIII, the AO framework converges within only a few iterations, with  $T$  typically being much smaller than both  $M$  and  $N_\phi$ . Therefore, the practical computational burden of the proposed algorithm is primarily governed by the structural system parameters  $M$ ,  $N$ ,  $M_p$ , and  $N_\phi$ , rather than by iterative convergence, confirming the scalability and efficiency of the proposed design.

## VIII. SIMULATION RESULTS

### A. Simulation Setup

We evaluate the performance of the proposed FRIS configuration algorithm, where the system parameters are in Table II. Unless otherwise specified, we consider an FRIS-aided downlink system assisted by BS, FRIS, user located in  $(0, 0, 5)$  m,  $(10, 10, 5)$  m,  $(50, 0, 0)$  m, respectively. Each selected FRIS port applies a discrete phase-shifting coefficient

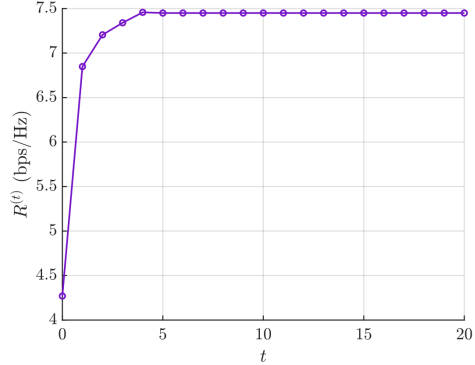


Fig. 5. Rate  $R^{(t)}$  according to iteration  $t$  under general codebook.

chosen from a finite unit-modulus codebook, where every  $w_m$  ( $w_m \in \mathcal{W}_m$ ) is uniformly selected from  $[0, 2\pi)$ . For performance verification, the achievable rate is evaluated as

$$R = \log_2 \left(1 + \frac{|z|^2}{\sigma^2}\right). \quad (65)$$

which is a strictly increasing function of  $|z|$  and hence any improvement in  $|z|$  directly translates into a monotonic increase in  $R$ . All reported results are averaged over  $10^3$  independent channel realizations, and we evaluate the average achievable rate  $\mathbb{E}[R]$ . For optimality-verification plots, we additionally consider the normalized beamforming-gain ratio

$$\Delta_G \triangleq \frac{|z|}{|z_{\text{opt}}|}, \quad (66)$$

where  $z_{\text{opt}}$  corresponds to the globally optimal solution obtained via exhaustive search of  $M_o$  FRIS ports among  $M$  candidates. Due to the exponential complexity of brute-force search,  $\Delta_G$  is evaluated for  $M = 5$  and  $M_o \leq 4$ .

We compare the proposed algorithm with two benchmark schemes, where  $\mathbf{f}_B$  is determined by same means of the proposed framework. In the “random ports” scheme,  $\Gamma^*$  is selected uniformly at random from all  $\binom{M}{M_o}$  possibilities. For the selected ports,  $\{w_m^*\}_{m \in \Gamma^*}$  are chosen by  $w_m^* = \arg d - \arg h_m$  ( $\forall m \in \Gamma^*$ ) [18], [34]. In the “Top- $|h|$  Ports” scheme, the  $M_o$  ports with the largest  $|h_m|$  are deterministically selected to form  $\Gamma^*$ , and the corresponding  $\{w_m^*\}_{m \in \Gamma^*}$  are determined in the same quantized phase-alignment manner as in the random-port benchmark.

Fig. 5 illustrates the convergence behavior of the proposed framework by showing the evolution of the achievable rate  $R^{(t)}$  with respect to the iteration index  $t$ . Herein,  $R^{(t)}$  increases rapidly and reaches saturation within only a few iterations, indicating fast convergence; which concludes that  $T$  in Section VII remains very small, typically on the order of fewer than ten iterations. This trend is consistent with the theoretical properties of the proposed AO procedure, in which each iteration monotonically improves (or preserves) the objective value. The minor fluctuations observed around the converged value stem from the discrete FRIS port selection and phase quantization, but their impact is negligible, thereby confirming the stability and efficiency of the proposed algorithm.

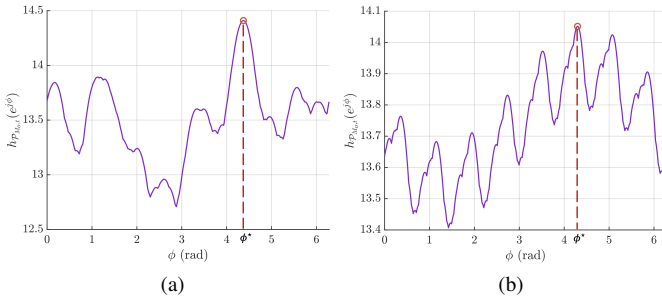


Fig. 6.  $h_{\mathcal{P}_{M_o,t}}(e^{j\phi})$  according to  $\phi \in [0, 2\pi]$  with (a) general and (b) regular  $M_p$ -gon codebook.

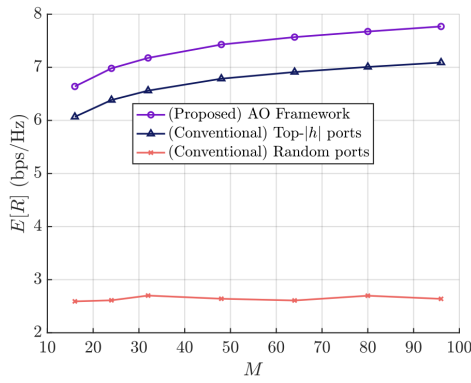


Fig. 7.  $\mathbb{E}[R]$  according to  $M$  under general codebook.

Fig. 6 illustrates  $h_{\mathcal{P}_{M_o,t}}(e^{j\phi})$  as a function of  $\phi$ . In the case of a general finite codebook in Fig. 6a,  $h_{\mathcal{P}_{M_o,t}}(e^{j\phi})$  exhibits an irregular but continuous profile, reflecting the combined effect of port selection and discrete phase adaptation across directions. By contrast, under a regular  $M_p$ -gon codebook in Fig. 6b, it becomes more regular and structured due to uniform phase quantization and its closed-form cosine structure in (49). Herein, within each interval where  $\Gamma^*(\phi)$  and  $k_m^*(\phi)$  remain unchanged, the function reduces to a smooth sum of cosine terms and admits at most one stationary point. Non-smooth points occur only at a finite number of breakpoints induced by  $\Phi^{\text{br}}$ , which correspond to the visible kinks in Fig. 6. In both cases,  $\phi^*$  corresponds to the global maximum of  $h_{\mathcal{P}_{M_o,t}}(e^{j\phi})$ , which directly determines the optimal FRIS configuration. This observation validates the proposed one-dimensional directional search and highlights how finite phase codebooks shape the geometry of the support function.

Fig. 7 illustrates  $\mathbb{E}[R]$  as a function of  $M$ . As  $M$  increases,  $\mathbb{E}[R]$  improves monotonically for all schemes, since a larger candidate set provides more flexibility in selecting favorable FRIS ports. The proposed framework-based FRIS design benefits most from this increase, as it exploits the enlarged port pool to identify the Top- $M_o$  ports that maximize the support function, thereby achieving a higher coherent combining gain. In contrast, the random-port and Top- $|h|$  benchmarks rely on non-geometric or magnitude-only selection rules, which cannot fully utilize the increased spatial diversity. As a result, the performance gap between the proposed scheme and the

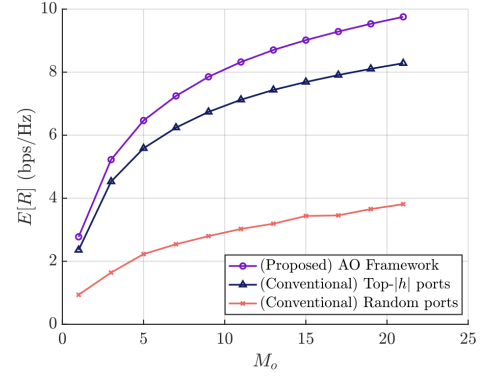


Fig. 8.  $\mathbb{E}[R]$  according to  $M_o$  under general codebook.

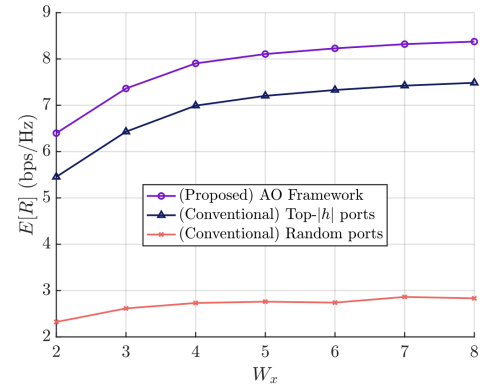


Fig. 9.  $\mathbb{E}[R]$  according to  $W_x$  under general codebook.

benchmarks becomes more pronounced as  $M$  grows. This is because increasing  $M$  enlarges the search space of candidate ports and thus creates more multiport combining opportunities, the proposed scheme can more effectively exploit the additional spatial DoF through joint port selection and quantized phase adaptation. In contrast, the benchmarks use either random selection or a myopic magnitude-based rule (i.e., Top- $|h|$ ), which cannot fully capture inter-port complementarity increases with  $M$ .

Fig. 8 shows  $\mathbb{E}[R]$  versus  $M_o$ . Increasing  $M_o$  leads to a consistent performance improvement, since more ports contribute constructively to  $z = d + \sum_{m \in \Gamma} h_m w_m$ . The proposed Minkowski-geometry-based framework achieves the largest gain by selecting the  $M_o$  ports with the highest  $s_m(\phi)$ , ensuring near-optimal coherent combining. By contrast, the Top- $|h|$  scheme does not explicitly account for phase alignment across ports, while the random-port scheme selects ports without considering their geometric contribution, resulting in noticeably lower performance, especially for larger  $M_o$ .

Fig. 9 illustrates  $\mathbb{E}[R]$  versus  $W_x$ . As  $W_x$  increases, the inter-element spacing grows and the spatial correlation among candidate ports decreases, providing richer location diversity and thus improving the beamforming gain. Accordingly,  $\mathbb{E}[R]$  increases and gradually saturates for sufficiently large  $W_x$ , since after  $d = \frac{\lambda}{2}$ -spacing, the spatial correlation characterized by  $j_0$ , which experiences its steepest decline around  $\frac{\lambda}{2}$  [37],

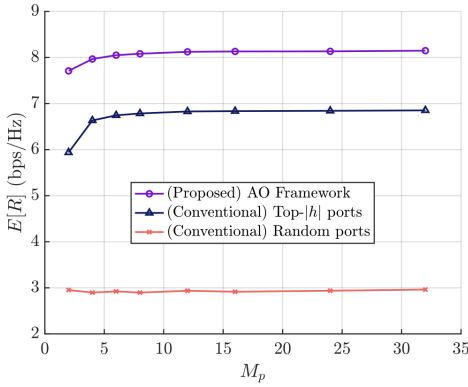


Fig. 10.  $\mathbb{E}[R]$  according to  $M_p$  under  $M_p$ -gon codebook.

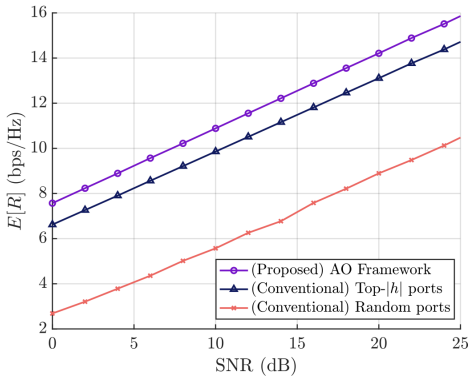


Fig. 11.  $\mathbb{E}[R]$  according to SNR under general codebook.

[40], [41], i.e.,  $W_x > 4$  ( $\because M_x = 8$ ), is already sufficiently mitigated. Herein, the proposed AO framework consistently achieves the highest rate, whereas the Top- $|h|$  and random-port benchmarks cannot fully exploit the additional spatial DoF.

Fig. 10 depicts the impact of  $M_p$  on  $\mathbb{E}[R]$  under a regular  $M_p$ -gon codebook. As  $M_p$  increases,  $\mathbb{E}[R]$  improves and gradually saturates. This behavior is explained by the reduction of phase-quantization error as  $M_p$  grows: finer phase resolution allows each FRIS port to better align its reflected signal with the optimal direction. According to (41) and (45),  $\delta_{M_p}$  decreases with  $M_p$ , leading to larger effective combining gains. Once the quantization error becomes sufficiently small, further increases in  $M_p$  yield diminishing returns, resulting in the observed saturation. Nevertheless, the proposed framework consistently outperforms the benchmarks, since it jointly optimizes port selection and quantized phase adaptation in a direction-aware manner based on Minkowski-sum-geometry of codebook spaces, whereas the benchmarks rely on heuristic or port-wise rules that cannot fully exploit the reduced quantization error even at high phase resolutions.

Fig. 11 presents  $\mathbb{E}[R]$  as a function of signal-to-noise ratio (SNR). Herein, the proposed framework consistently outperforms the benchmark schemes across the entire SNR range. This advantage stems from the joint optimization of beamforming and FRIS configuration, which maximizes  $|z|$  and thus preserves a strong array gain even at high SNR.

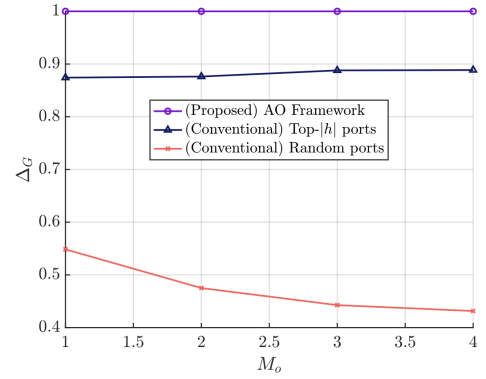


Fig. 12.  $\Delta_G$  according to  $M_o$  under general codebook.

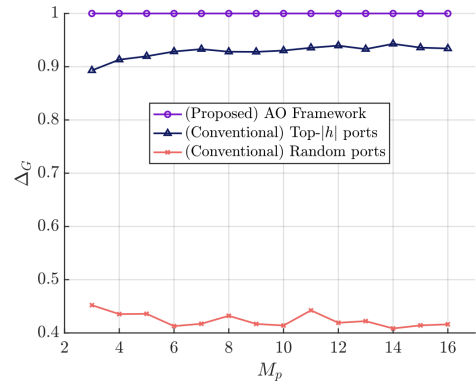


Fig. 13.  $\Delta_G$  according to  $M_p$  under  $M_p$ -gon codebook.

In contrast, the benchmark schemes suffer from suboptimal port selection or phase misalignment, leading to a persistent performance gap.

Fig. 12 shows  $\Delta_G$  versus  $M_o$  for general finite codebooks. The proposed scheme achieves values of  $\Delta_G$  close to one even for moderate  $M_o$ , indicating that it attains near-optimal performance compared to exhaustive search. This result confirms that the MRT and the Minkowski-geometry-based formulation effectively captures the essential structure of the optimal FRIS configuration. In contrast, the benchmark schemes exhibit significantly lower  $\Delta_G$ , as their heuristic port-selection strategies fail to account for the joint geometric contribution of multiple ports.

Fig. 13 illustrates  $\Delta_G$  as a function of  $M_p$  under a regular  $M_p$ -gon codebook. As  $M_p$  increases,  $\Delta_G$  rapidly approaches one, demonstrating that the proposed framework converges to the globally optimal solution as the phase resolution improves. Notably, near-optimal performance is achieved even for relatively small  $M_p$ , highlighting the robustness of the proposed design to coarse phase quantization. This observation confirms that the proposed framework can effectively operate under practical hardware constraints with limited phase resolution.

## IX. CONCLUSION

In this paper, we proposed a principled framework for beamforming-gain maximization in FRIS-assisted downlink

systems under multi-antenna BS and practical finite-resolution phase constraints. To tackle the resulting mixed discrete optimization, an AO framework was developed that combines a closed-form MRT update at the BS with a Minkowski-geometry-based reformulation of the FRIS configuration problem. By exploiting the geometric structure of the reflected-sum codebook space, the FRIS subproblem was reduced to a one-dimensional maximization of a support function, enabling efficient configuration via direction-dependent per-port scoring, Top- $M_o$  port selection, and optimal quantized phase assignment. For the practically important case of regular  $M_p$ -gon phase-shifter codebooks, we further revealed a piecewise-smooth structure of the resulting support function and developed a finite candidate-angle maximization procedure that provably identifies the global optimum by evaluating only a finite set of critical angles, thereby avoiding exhaustive one-dimensional search. Simulation results demonstrated consistent performance gains over benchmark schemes, near-optimality with respect to exhaustive search, accurate identification of the optimal phase via support-function maximization, and fast, stable convergence. Overall, the proposed framework provides an efficient and geometry-driven solution for FRIS-aided wireless networks and offers a solid foundation for extensions to more general FRIS architectures in 6G systems.

## REFERENCES

- [1] M. Giordani *et al.*, “Toward 6G networks: Use cases and technologies,” *IEEE Commun. Mag.*, vol. 58, no. 3, pp. 55–61, Mar. 2020.
- [2] G. Gui *et al.*, “6G: Opening new horizons for integration of comfort, security and intelligence,” *IEEE Wireless Commun.*, pp. 1–7, Oct. 2020.
- [3] B. Smida *et al.*, “Full-duplex wireless for 6G: Progress brings new opportunities and challenges,” *IEEE J. Sel. Areas Commun.*, vol. 41, no. 9, pp. 2729–2750, Sep. 2023.
- [4] D. Gündüz *et al.*, “Beyond transmitting bits: Context, semantics, and task-oriented communications,” *IEEE J. Sel. Areas Commun.*, vol. 41, no. 1, pp. 5–41, Jan. 2023.
- [5] Y. Kim *et al.*, “A state-of-the-art survey on full-duplex network design,” *Proc. IEEE*, vol. 112, no. 5, pp. 463–486, May 2024.
- [6] Y. Wu *et al.*, “Massive access for future wireless communication systems,” *IEEE Wireless Commun.*, vol. 27, no. 4, pp. 148–156, Aug. 2020.
- [7] H.-J. Moon and C.-B. Chae, “Cooperative ground-satellite scheduling and power allocation for urban air mobility networks,” *IEEE J. Sel. Areas Commun.*, vol. 43, no. 1, pp. 218–233, Jan. 2025.
- [8] H.-J. Moon *et al.*, “AI-based beam management for FR3 FDD MIMO via online channel synthesis,” *IEEE J. Sel. Areas Commun.*, pp. 1–1, 2026.
- [9] M. Di Renzo *et al.*, “Smart radio environments empowered by reconfigurable intelligent surfaces: How it works, state of research, and the road ahead,” *IEEE J. Sel. Areas Commun.*, vol. 38, no. 11, pp. 2450–2525, Nov. 2020.
- [10] C. You *et al.*, “Enabling smart reflection in integrated air-ground wireless network: IRS meets UAV,” *IEEE Wireless Commun. Mag.*, vol. 28, no. 6, pp. 138–144, Dec. 2021.
- [11] G. Alexandopoulos *et al.*, “RIS-enabled smart wireless environments: deployment scenarios, network architecture, bandwidth and area of influence,” *Eurasip Jour. Wireless Commun. and Netw.*, vol. 203, no. 1, p. 103, Oct. 2023.
- [12] Q. Wu *et al.*, “Intelligent reflecting surface-aided wireless communications: A tutorial,” *IEEE Trans. Commun.*, vol. 69, no. 5, pp. 3313–3351, May 2021.
- [13] E. Basar and H. V. Poor, “Present and future of reconfigurable intelligent surface-empowered communications [perspectives],” *IEEE Signal Process. Mag.*, vol. 38, no. 6, pp. 146–152, Nov. 2021.
- [14] Z. Wan *et al.*, “Terahertz massive MIMO with holographic reconfigurable intelligent surfaces,” *IEEE Trans. Commun.*, vol. 69, no. 7, pp. 4732–4750, Jul. 2021.
- [15] D. Jun *et al.*, “Resource-efficient near-field misfocus mitigation in ris-assisted wideband multi-user systems,” *IEEE Trans. Cogn. Commun. Netw.*, vol. 12, pp. 3148–3163, 2026.
- [16] M. Di Renzo *et al.*, “Reconfigurable intelligent surfaces vs. relaying: Differences, similarities, and performance comparison,” *IEEE Open J. Commun. Soc.*, vol. 1, pp. 798–807, Jun. 2020.
- [17] H.-B. Jeon and C.-B. Chae, “Ampli-flection for 6G: Active-RIS-aided aerial backhaul with full 3D coverage,” *arXiv:2601.17751*, 2026.
- [18] E. Björnson *et al.*, “Intelligent reflecting surface versus decode-and-forward: How large surfaces are needed to beat relaying?” *IEEE Wireless Commun. Lett.*, vol. 9, no. 2, pp. 244–248, Feb. 2020.
- [19] H.-B. Jeon *et al.*, “An energy-efficient aerial backhaul system with reconfigurable intelligent surface,” *IEEE Trans. Wireless Commun.*, vol. 21, no. 8, pp. 6478–6494, Aug. 2022.
- [20] A. Salem *et al.*, “A first look at the performance enhancement potential of fluid reconfigurable intelligent surface,” *arXiv:2502.17116v1*, 2025.
- [21] H. Xiao *et al.*, “From fixed to fluid: Unlocking the new potential with fluid RIS (FRIS),” *arXiv:2509.18899*, 2025.
- [22] K.-K. Wong *et al.*, “Fluid antenna systems,” *IEEE Trans. Wireless Commun.*, vol. 20, no. 3, pp. 1950–1962, Mar. 2021.
- [23] K.-K. Wong and K.-F. Tong, “Fluid antenna multiple access,” *IEEE Trans. Wireless Commun.*, vol. 21, no. 7, pp. 4801–4815, Jul. 2022.
- [24] W. K. New *et al.*, “Fluid antenna systems: Redefining reconfigurable wireless communications,” *IEEE J. Sel. Areas Commun.*, vol. 44, pp. 1013–1044, 2026.
- [25] M. R. Castellanos *et al.*, “Embracing reconfigurable antennas in the tri-hybrid MIMO architecture for 6G and beyond,” *IEEE Trans. Commun.*, vol. 74, pp. 381–401, 2026.
- [26] R. W. Heath *et al.*, “The tri-hybrid MIMO architecture,” *IEEE Wireless Commun.*, vol. 33, no. 1, pp. 199–206, Feb. 2026.
- [27] H. Xiao *et al.*, “Fluid reconfigurable intelligent surfaces: joint on-off selection and beamforming with discrete phase shifts,” *IEEE Wireless Commun. Lett.*, vol. 14, no. 10, pp. 3124–3128, Oct. 2025.
- [28] X. Zhu *et al.*, “Fluid reconfigurable intelligent surface (FRIS) enabling secure wireless communications,” *arXiv:2511.15860*, 2025.
- [29] F. Ghadi *et al.*, “Performance analysis of wireless communication systems assisted by fluid reconfigurable intelligent surfaces,” *IEEE Wireless Commun. Lett.*, vol. 14, no. 12, pp. 3922–3926, Dec. 2025.
- [30] M. Kaveh *et al.*, “Ambient backscatter communication assisted by fluid reconfigurable intelligent surfaces,” *arXiv:2510.24725*, 2026.
- [31] ———, “Physical layer security over fluid reconfigurable intelligent surface-assisted communication systems,” *arXiv:2509.24845*, 2025.
- [32] H. Xiao *et al.*, “Fluid reconfigurable intelligent surface with element-level pattern reconfigurability: Beamforming and pattern co-design,” vol. 25, pp. 10 791–10 806, Jan. 2026.
- [33] S. Ren *et al.*, “A linear time algorithm for the optimal discrete IRS beamforming,” *IEEE Wireless Commun. Lett.*, vol. 12, no. 3, pp. 496–500, Mar. 2023.
- [34] Q. Wu and R. Zhang, “Intelligent reflecting surface enhanced wireless network via joint active and passive beamforming,” *IEEE Trans. Wireless Commun.*, vol. 18, no. 11, pp. 5394–5409, Nov. 2019.
- [35] H. Do and A. Lozano, “Optimum discrete beamforming via Minkowski sum of polygons,” *arXiv:2512.15546*, 2025.
- [36] ———, “Beamforming gain with nonideal phase shifters,” *arXiv:2601.09426*, 2026.
- [37] M. Abramowitz and I. A. Stegun, *Handbook of Mathematical Functions with Formulas, Graphs, and Mathematical Tables*. National Bureau of Standards, 1964.
- [38] S. Boyd and L. Vandenberghe, *Convex Optimization*. Cambridge, UK: Cambridge Univ. Press, 2004.
- [39] R. Schneider, *Convex Bodies: The Brunn-Minkowski Theory*. Cambridge University Press, 1993.
- [40] K. K. Wong *et al.*, “Performance limits of fluid antenna systems,” *IEEE Commun. Lett.*, vol. 24, no. 11, pp. 2469–2472, Nov. 2020.
- [41] D.-S. Shiu *et al.*, “Fading correlation and its effect on the capacity of multielement antenna systems,” *IEEE Trans. Commun.*, vol. 48, no. 3, pp. 502–513, Mar. 2000.